Progress In Electromagnetics Research M, Vol. 45, 83–90, 2016

Fast Algorithm of Wideband Electromagnetic Scattering of Homogeneous Dielectric Targets

Bo Zhao*, Shu-Xi Gong, Xing Wang, and Yu Zhang

Abstract—The PMCHWT-IE-FFT-BURA is applied to the wideband analysis of electromagnetic scattering property of homogeneous targets. Over the broad frequency band, the fast computation is achieved by the Maehly expansion on the basis of the Chebyshev approximation of the electric and magnetic currents. On the Chebyshev sampling points, PMCHWT-IE-FFT greatly reduces the memory requirement by sparsely storing the impedance matrix and decreases the computational time to the greatest degree by block acceleration of the matrix-vector product. Finally, numerical results show that the proposed method can make efficient analysis of wideband property of homogeneous targets without sacrificing accuracy much .

1. INTRODUCTION

The electromagnetic scattering property of homogeneous targets [1] possesses theoretical meaning and practical value in the fields of target identification, wave propagation in complex environment and resources exploration. In computational electromagnetics (CEM), the method of moments (MoM) [2] is an effective tool for its high accuracy. However, for the wideband computation of homogeneous targets, one-by-one frequency point has to be computed by the MoM within the bandwidth, which makes the process prohibitively long. Consequently, the fast frequency sweeping technique of homogeneous targets is of great significance.

Since the end of 1960s, great achievements have been made in the MoM research. However, the conventional MoM has to save the dense impedance matrix, so its performance is limited by the hardware resources. Under this circumstance, more and more attention has been focused on fast algorithms such as MLFMA [3, 4], AIM [5, 6] and IE-FFT [7–9]. The PMCHWT-IE-FFT involved in this paper is different from the previous PEC situation. The surface of the homogeneous targets contains not only equivalent electric currents, but also magnetic currents. This means that for the target meshed by triangular patches, two RWG basis functions [10] are needed to simulate the electric and magnetic currents, respectively, on a pair of triangles sharing the common edge. This also leads to the fact that the number of unknowns of homogeneous targets is more than twice as that of the PEC case of the same electrical size. In addition, the impedance matrix arising from the PMCHWT-MoM obtains the form of two-by-two submatrices which can be utilized to get the maximum reduction of CPU time by block acceleration with the FFT.

For the purpose of accurate and efficient analysis of broadband scattering property, the Asymptotic Waveform Evaluation (AWE) [11, 12], Model Based Parameter Estimation (MBPE) [13], Best Uniform Rational Approximation (BURA) [14–16] and other methods are proposed one after another. In the above methods, both the AWE and MBPE need to calculate and store higher derivatives of the

Received 12 November 2015, Accepted 8 December 2015, Scheduled 18 December 2015

* Corresponding author: Bo Zhao (m15991342657@163.com).

The authors are with the National Key Laboratory of Antennas and Microwave Technology, Xidian University, Xi'an, Shaanxi 710071, China.

impedance matrix. On the contrary, the BURA is welcomed by scholars for memory saving and easy combination with the existing codes.

In this paper, the PMCHWT-IE-FFT united with the BURA has firstly been applied to the broadband analysis of the EM scattering of the homogeneous targets. First of all, the procedure is carried out by selecting a group of Chebyshev nodes within the bandwidth. Secondly, PMCHWT-IE-FFT is performed to compute the electric and magnetic currents over these Chebyshev nodes. Thirdly, the coefficients of the Chebyshev polynomials can be achieved on the basis of the last step. Lastly, the electric and magnetic currents of arbitrary frequency over the given bandwidth can be obtained via the Maehly Approximation.

2. THEORY AND FORMULATIONS

2.1. PMCHWT-IE-FFT

Consider a homogeneous targets with permittivity of $\varepsilon(\mathbf{r}) = \varepsilon_0\varepsilon_r(\mathbf{r})$ and permeability of μ_0 (non-magnetic material) in free space which is illuminated by plane wave ($\mathbf{E}^{inc}$, $\mathbf{H}^{inc}$), as shown in Fig. 1. The surface of the targets is denoted by S. The PMCHWT equations resulting from the homogeneous bodies are shown as below

$$[L_1(\mathbf{J}) + L_2(\mathbf{J}) + K_1(\mathbf{M}) + K_2(\mathbf{M})]_{\tan} = \mathbf{E}^{inc}\big|_{\tan} \tag{1}$$

$$\left[-K_1(\mathbf{J}) - K_2(\mathbf{J}) + \frac{1}{\eta_1^2}L_1(\mathbf{M}) + \frac{1}{\eta_2^2}L_2(\mathbf{M})\right]_{\tan} = \mathbf{H}^{inc}\big|_{\tan} \tag{2}$$

where $\mathbf{J}$ and $\mathbf{M}$ represent the equivalent surface electric and magnetic currents, respectively. $L_j(\mathbf{X})$ denotes the operator L of EFIE while $K_j(\mathbf{X})$ signifies the operator K of MFIE. Following the process of expansion of electric and magnetic currents by the RWG basis function and Galerkin test, the PMCHWT equation can be arranged as below,

$$\begin{bmatrix} \mathbf{Z}^{JJ} & \mathbf{Z}^{JM} \\ \mathbf{Z}^{MJ} & \mathbf{Z}^{MM} \end{bmatrix} \begin{bmatrix} \mathbf{I} \\ \mathbf{P} \end{bmatrix} = \begin{bmatrix} \mathbf{V}^{J} \\ \mathbf{V}^{M} \end{bmatrix} \tag{3}$$

where $\mathbf{I}$ and $\mathbf{P}$ are the coefficient vectors of RWG expansion; $\mathbf{V}^J$ and $\mathbf{V}^M$ are the excitation vectors arising from the electric and magnetic component of the incident plane wave; $\mathbf{Z}^{JJ}$, $\mathbf{Z}^{JM}$, $\mathbf{Z}^{MJ}$ and $\mathbf{Z}^{MM}$ are the submatrices of the impedance matrix. The elements of $\mathbf{Z}^{JJ}$ and $\mathbf{Z}^{MM}$ all contain operator L of regions 1 and 2 while $\mathbf{Z}^{JM}$ and $\mathbf{Z}^{MJ}$ comprise operator K of regions 1 and 2.

Initially, the PMCHWT-IE-FFT requires constructing a cuboid which physically embraces the homogeneous targets. The Cartesian grids on the cuboid are established, as displayed in Fig. 2, and the total number of the grids is supposed as N_g. The Green function of free space $G(k_j)$ is interpolated by the Lagrange polynomials, which leads to two benefits. The first one is that the separation of source point and field point will facilitate the approximation of far-field elements of the impedance matrix.

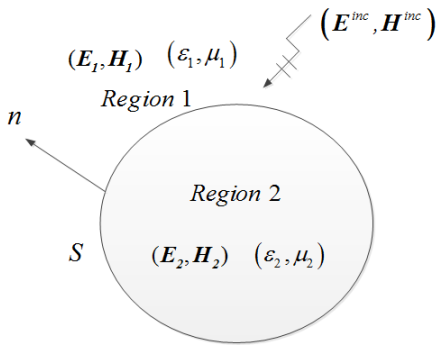

Figure 1. Homogeneous target and its equivalent model.

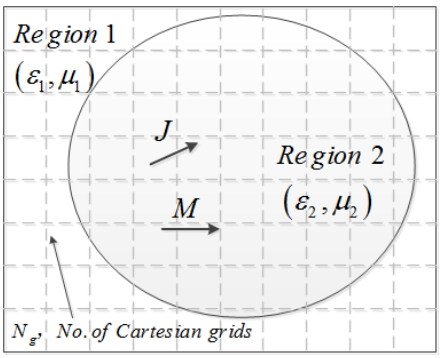

Figure 2. Cartesian Grids of the PMCHWT-IE-FFT.

The second one is that the obtained matrix of discrete Green function $\mathbf{g}(k_j)$ is provided with the 3-layer Toeplitz property which is the foundation of the FFT acceleration of matrix-vector product. Therefore, it can be concluded from Eq. (3) that each matrix of discrete Green function of all the four submatrices possesses the 3-layer Toeplitz property. In the following, the expressions of submatrix-vector product by FFT acceleration are given.

$$\begin{aligned}\mathbf{Z}_{IE\text{-}FFT}^{JJ,far}\mathbf{I} &= \vec{\prod}_A F^{-1}\left[F\left(\mathrm{j}k_1\eta_1\tilde{\mathbf{g}}_1+\mathrm{j}k_2\eta_2\tilde{\mathbf{g}}_2\right)F\left(\vec{\prod}_A^T\mathbf{I}\right)\right]\\ &\quad -\prod_D F^{-1}\left[F\left(\frac{\mathrm{j}\eta_1}{k_1}\tilde{\mathbf{g}}_1+\frac{\mathrm{j}\eta_2}{k_2}\tilde{\mathbf{g}}_2\right)F\left(\prod_D^T\mathbf{I}\right)\right] \quad (4)\\ \mathbf{Z}_{IE\text{-}FFT}^{JM,far}\mathbf{P} &= \eta_0\vec{\prod}_M F^{-1}\left[F\left(\tilde{\mathbf{g}}_1+\tilde{\mathbf{g}}_2\right)F\left(\vec{\prod}_A^T\mathbf{P}\right)\right] \quad (5)\\ \mathbf{Z}_{IE\text{-}FFT}^{MJ,far}\mathbf{I} &= -\eta_0\vec{\prod}_M F^{-1}\left[F\left(\tilde{\mathbf{g}}_1+\tilde{\mathbf{g}}_2\right)F\left(\vec{\prod}_A^T\mathbf{I}\right)\right] \quad (6)\\ \mathbf{Z}_{IE\text{-}FFT}^{MM,far}\mathbf{P} &= \vec{\prod}_A F^{-1}\left[F\left(\frac{\mathrm{j}k_1\eta_0^2}{\eta_1}\tilde{\mathbf{g}}_1+\frac{\mathrm{j}k_2\eta_0^2}{\eta_2}\tilde{\mathbf{g}}_2\right)F\left(\vec{\prod}_A^T\mathbf{P}\right)\right]\\ &\quad -\prod_D F^{-1}\left[F\left(\frac{\mathrm{j}\eta_0^2}{\eta_1k_1}\tilde{\mathbf{g}}_1+\frac{\mathrm{j}\eta_0^2}{\eta_2k_2}\tilde{\mathbf{g}}_2\right)F\left(\prod_D^T\mathbf{P}\right)\right] \quad (7)\end{aligned}$$

where F and F^{-1} designate the fast Fourier transformation and inverse fast Fourier transformation, respectively. $\tilde{\mathbf{g}}_i$ is an indication of the first column of circular matrix expanded from $\mathbf{g}(k_i)$, $\mathrm{i}=1,2$. $\vec{\prod}_A$, $\prod_D$ and $\vec{\prod}_M$, respectively, represent the transformation matrix of the electric vector potential, electric scalar potential and magnetic vector potential. The dimensions of the three transformation matrices are all N-by-N_g while the length of the unknown vector $\mathbf{I}$ or $\mathbf{P}$ is N.

$$\vec{\prod}_A = \iint_S \left(\begin{array}{cccc}\mathbf{f}_1 & \mathbf{f}_2 & \ldots & \mathbf{f}_N\end{array}\right)^T \left(\begin{array}{cccc}\beta_1^p & \beta_2^p & \ldots & \beta_{N_g}^p\end{array}\right) ds \quad (8)$$

$$\prod_D = \iint_S \left(\begin{array}{cccc}\nabla\cdot\mathbf{f}_1 & \nabla\cdot\mathbf{f}_2 & \ldots & \nabla\cdot\mathbf{f}_N\end{array}\right)^T \left(\begin{array}{cccc}\beta_1^p & \beta_2^p & \ldots & \beta_{N_g}^p\end{array}\right) ds \quad (9)$$

$$\vec{\prod}_M = \iint_S \left(\begin{array}{cccc}\mathbf{f}_1 & \mathbf{f}_2 & \ldots & \mathbf{f}_N\end{array}\right)^T \times \left(\begin{array}{cccc}\nabla\beta_1^p & \nabla\beta_2^p & \ldots & \nabla\beta_{N_g}^p\end{array}\right) ds \quad (10)$$

2.2. PMCHWT-IE-FFT-BURA

Since the impedance matrix and excitation vector in the MoM are the function of frequency, the wideband computation of homogeneous targets necessitates repeated filling and solving of Eq. (11) at each frequency point, which is pretty time-consuming.

$$\left[\begin{array}{cc}\mathbf{Z}^{JJ}(k) & \mathbf{Z}^{JM}(k)\\ \mathbf{Z}^{MJ}(k) & \mathbf{Z}^{MM}(k)\end{array}\right]\left[\begin{array}{c}\mathbf{I}(k)\\ \mathbf{P}(k)\end{array}\right] = \left[\begin{array}{c}\mathbf{V}^{J}(k)\\ \mathbf{V}^{M}(k)\end{array}\right] \quad (11)$$

To begin with, the BURA technique chooses a set of Chebyshev nodes $k_j (j=0,1,\ldots,Q)$ over the given bandwidth $[k_a, k_b]$ abiding by Eq. (12),

$$k_j = \frac{1}{2}\left[\tilde{k}_j\left(k_b-k_a\right)+\left(k_a+k_b\right)\right] \quad (12)$$

where $\tilde{k}_j$ represents the normalized transformation coefficients of wavenumber k over the known bandwidth. The formulation of $\tilde{k}_j$ is given below,

$$\tilde{k}_j = \cos\left(\frac{2j+1}{2(n+1)}\pi\right) \quad (13)$$

Afterwards, the $\vec{\prod}_A$, $\prod_D$ and $\vec{\prod}_M$ regarding the obtained set of RWG basis function are computed. The FFT operations for the first column of circular matrix resulting from the 3-layer Toeplitz matrix $\mathbf{g}(k_i),\ i = 1, 2$ are carried out. The corrected near-field elements of the submatrices $\mathbf{Z}^{JJ}(k_j)$, $\mathbf{Z}^{JM}(k_j)$, $\mathbf{Z}^{MJ}(k_j)$ and $\mathbf{Z}^{MM}(k_j)$ are calculated and saved. On getting these basic data, the electric and magnetic currents $\mathbf{I}$ and $\mathbf{P}$ at the Chebyshev nodes k_j can be resolved iteratively according to the Eqs. (4)–(7). Next step will be the computing process of the expansion coefficients of the Chebyshev polynomials for the whole bandwidth, i.e., $c_{2n,l}$.

$$c_{2n,l} = \frac{2}{Q+1} \sum_{j=0}^{Q} \begin{bmatrix} I_n(k_j) \\ P_n(k_j) \end{bmatrix} T_l(\tilde{k}_j) \tag{14}$$

where $T_l(x)$ is the Chebyshev polynomial. With $c_{2n,l}$, the electric and magnetic currents at any frequency within the bandwidth can be preliminarily expressed as below,

$$\begin{bmatrix} I_n(k) \\ P_n(k) \end{bmatrix} = \begin{bmatrix} I_n \\ P_n \end{bmatrix} \left(\frac{\tilde{k}(k_b - k_a) + (k_a + k_b)}{2} \right) \approx \sum_{l=0}^{Q} c_{2n,l} T_l(\tilde{k}) - \frac{c_{2n,0}}{2} \tag{15}$$

In Eq. (15), $\tilde{k}$ is the normalized transformation coefficient of k. The relationship between $\tilde{k}$ and k conforms to Eq. (12). Finally, the Meahly approximation is employed to improve the accuracy of $\mathbf{I}$ and $\mathbf{P}$.

$$\begin{bmatrix} I_n(k) \\ P_n(k) \end{bmatrix} \approx \frac{P_L(\tilde{k})}{Q_M(\tilde{k})} = \frac{\sum_{i=0}^{L} a_{2n,i} T_i(\tilde{k})}{1 + \sum_{j=1}^{M} b_{2n,j} T_j(\tilde{k})} \tag{16}$$

In the above equation, $a_{2n,i} (i = 0, 1, 2, \ldots, L)$ and $b_{2n,j} (j = 0, 1, 2, \ldots, M)$ can be achieved with the following formulae,

$$\begin{cases} a_{2n,0} = \dfrac{1}{2} \sum_{j=1}^{M} b_{2n,j} c_{2n,j} + \dfrac{1}{2} b_{2n,0} c_{2n,0} \\ a_{2n,i} = \sum_{j=1}^{M} \dfrac{1}{2} b_{2n,j} (c_{2n,|i-j|} + c_{2n,i+j}) + b_{2n,0} c_{2n,i} \quad i = 1, 2, ..., L \end{cases} \tag{17}$$

$$\begin{bmatrix} c_{2n,L+2} + c_{2n,L} & c_{2n,L+3} + c_{2n,L-1} & \cdots & c_{2n,L+M+1} + c_{2n,L-M+1} \\ c_{2n,L+3} + c_{2n,L+1} & c_{2n,L+4} + c_{2n,L} & \cdots & c_{2n,L+M+2} + c_{2n,L-M+2} \\ \vdots & \vdots & \ddots & \vdots \\ c_{2n,L+M+1} + c_{2n,L+M-1} & c_{2n,L+M+2} + c_{2n,L+M-2} & \cdots & c_{2n,L+2M} + c_{2n,L} \end{bmatrix} \begin{bmatrix} b_{2n,1} \\ b_{2n,2} \\ \vdots \\ b_{2n,M} \end{bmatrix}$$

$$= -2 \begin{bmatrix} c_{2n,L+1} \\ c_{2n,L+2} \\ \vdots \\ c_{2n,L+M} \end{bmatrix} \tag{18}$$

In order to evidently display the whole analytical process, Fig. 3 gives the sequence of the proposed technique.

3. NUMERICAL EXAMPLES AND ANALYSIS

To demonstrate the efficiency and accuracy of the PMCHWT-IE-FFT-BURA, three numerical examples are displayed with the incident plane wave propagating along $-z$ axis and polarized along x axis. The program codes of Fortran are implemented on a 2.0 GHz workstation with 32G memory. All the data

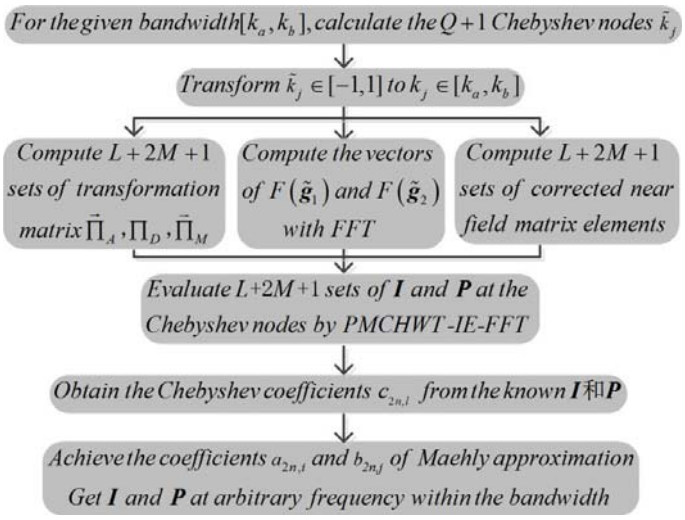

Figure 3. The flow chart of PMCHWT-IE-FFT-BURA.

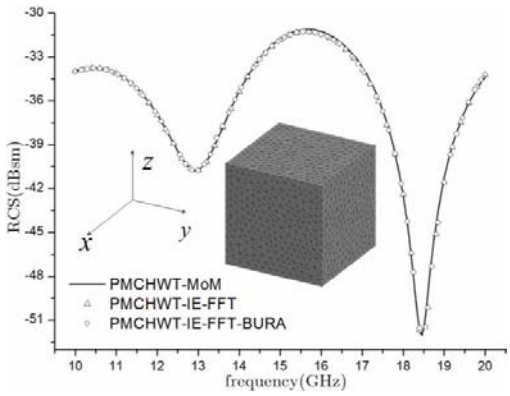

Figure 4. Broadband monostatic RCS of cuboid over 10–20 GHz.

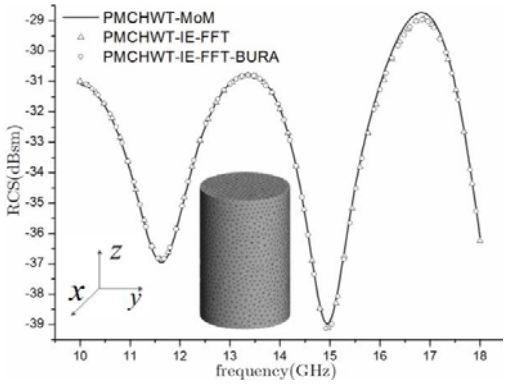

Figure 5. Broadband monostatic RCS of cylinder over 10–18 GHz.

are saved by double precision, and the GMRES is adopted as solver. In the PMCHWT-IE-FFT, $0.08\lambda_g$ is chosen as the Cartesian grid space and 2 selected as the order of Lagrange interpolating polynomials.

In the first example, we consider a homogeneous cuboid with edge-length of 1.8 cm and permittivity of 2.0. The cuboid is meshed into 3058 triangles which form 9174 unknowns. Fig. 4 shows the broadband monostatic RCS of the target as a function against frequency over the range from 10 to 20 GHz with an interval of 50 MHz in XOZ plane. The solid line indicates the result tackled by the conventional MoM while the triangle line implies the solution of PMCHWT-IE-FFT by means of one by one frequency point. It can be seen that the proposed technique, namely PMCHWT-IE-FFT-BURA, with $L = M = 6$ agrees well with the PMCHWT-MoM and PMCHWT-IE-FFT, which illustrates the accuracy of the proposed method in this paper.

The second example gives a cylinder whose permittivity is 2.2. The radius and height of the cylinder are fixed at 1.0 cm and 3.0 cm, respectively, and it is meshed into 4354 triangles and 13062 unknowns. Fig. 5 displays the wideband scattering property over 10–18 GHz with step of 40 MHz in XOZ plane. Likewise, we can find that the PMCHWT-IE-FFT-BURA ($L = M = 7$) maintains good precision compared with the other two.

The third example is about the investigation on cuboid of irregular shape with permittivity 2.25. The dimensions of the irregular cuboid are displayed in Fig. 6. The body is discretized into 4060 triangles and 12180 unknowns. The wideband monostatic RCS over 20–30 GHz with step of 50 MHz in XOZ

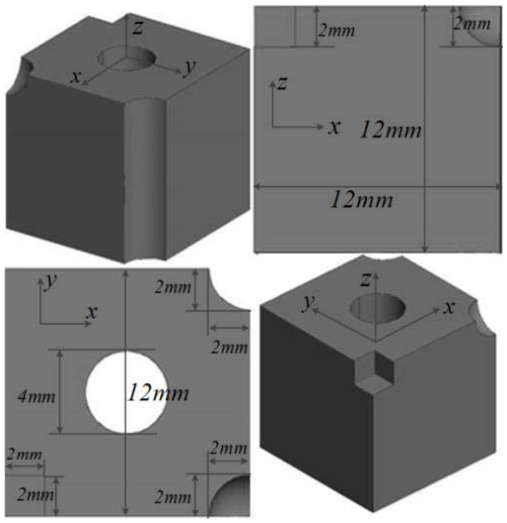

Figure 6. The dimensions of the irregular cuboid.

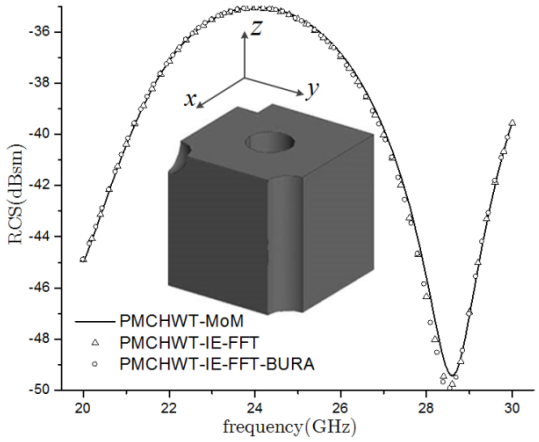

Figure 7. Broadband monostatic RCS of irregular cuboid over 20–30 GHz.

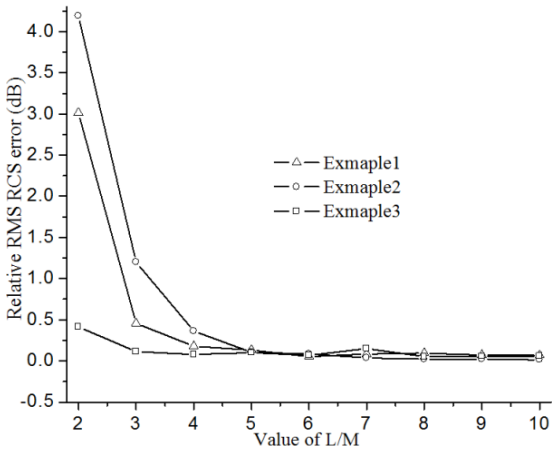

Figure 8. The RMS error of the proposed method versus L or M.

Table 1. Total CPU time of wideband RCS computation of example 1, example 2 and example 3.

Problem	No. of unknowns	No. of Frequency points	Total CPU Time (hour/min)		
			PMCHWT-MoM	PMCHWT-IE-FFT	PMCHWT-IE-FFT-BURA
Cuboid	9174	201	39/17	10/3	0/55
Cylinder	13062	201	91/22	22/6	2/26
Irregular cuboid	12180	201	118/43	26/39	3/33

plane is shown in Fig. 7, and good agreement is achieved among the PMCHWT-MoM, PMCHWT-IE-FFT and PMCHWT-IE-FFT-BURA ($L = M = 8$).

Taking the results of PMCHWT-IE-FFT as a benchmark, Fig. 8 reveals the variation of root mean square (RMS) error of PMCHWT-IE-FFT-BURA with the value of L or M. It can clearly be concluded that the precision is raised rapidly with the increase of L/M.

Table 1 manifests the total CPU time of the related method used in Figs. 4, 5 and 7 regarding the three numerical examples. The table reveals that aiming at the broadband RCS computing of homogeneous targets, the PMCHWT-IE-FFT-BURA can greatly boost the computational efficiency. In comparison with PMCHWT-IE-FFT and PMCHWT-MoM, the efficiency of the proposed technique is improved up to 90.9% and 97.7% in example 1, 89.0% and 97.3% in example 2, and 86.7% and 97.0% in example 3.

4. CONCLUSION

This paper presents a fast wideband algorithm for the homogeneous target, which closely unites PMCHWT-IE-FFT and BURA. To start with, the block characteristic of the impedance matrix due to PMCHWT-MoM is described. With this feature, block acceleration of FFT is applied to the PMCHWT-MoM to shorten the solving process at the Chebyshev nodes. On the basis of the previous steps, the RCS over the whole bandwidth can be obtained by the BURA. Numerical examples testify the efficiency and accuracy of the proposed method.

ACKNOWLEDGMENT

This work is supported by the National High Technology Research and Development Program of China (863 Program) (No. 2012AA01A308), National Natural Science Foundation of China (Nos. 61401327, 61201018, 61471278, 61501343), Program for New Century Excellent Talents in University of China (No. NCET-13-0949), Shaanxi Youth Science and Technology Star Project (No. 2013KJXX-67).

REFERENCES

1. Umashankar, K., A. Taflove, and S. M. Rao, "Electromagnetic scattering by arbitrary shaped three-dimensional homogeneous lossy dielectric objects," *IEEE Trans. Antennas Propag.*, Vol. 34, No. 6, 758–766, Jun. 1986
2. Zhang, Y., Z.-C. Lin, X.-W. Zhao, and T. K. Sarkar, "Performance of a massively parallel higher-order method of moments code using thousands of CPUs and its applications," *IEEE Trans. Antennas Propag.*, Vol. 62, No. 12, 6317–6324, Dec. 2014.
3. Song, J. M., C.-C. Lu, and W. C. Chew, "Multilevel fast multipole algorithm for electromagnetic scattering by large complex objects," *IEEE Trans. Antennas Propag.*, Vol. 45, No. 10, 1488–1493, Oct. 1997.
4. Man, M.-Y., Z.-Y. Lei, Y.-J. Xie, and Y.-Y. Wang, "Analysis of the electrical large scattering problem using the pre-corrected multilevel fast multipole algorithm," *Journal of Xidian University*, Vol. 39, No. 2, 133–137, 2012.
5. Bleszynski, E., M. Bleszynski, and T. Jaroszewicz, "AIM: Adaptive integral method for solving large-scale electromagnetic scattering and radiation problems," *Radio Sci.*, Vol. 31, No. 5, 1225–1251, Sep.–Oct. 1996.
6. Wang, X., S.-X. Gong, J. Ling, and X.-M. Wang, "Interpolation scheme based on adaptive integral method for solving electrically large radiation problem by surface/surface configuration," *Progress In Electromagnetics Research M*, Vol. 11, 203–211, 2010.
7. Seo. S. M. and J. F. Lee, "A fast IE-FFT algorithm for solving PEC scattering problems," *IEEE Trans. Magn.*, Vol. 41, No. 5, 1476–1479, May 2005.
8. An, X. and Z.-Q. Lü, "Application of IE-FFT with combined field integral equation to electrically large scattering problems," *Microw. Opt. Technol. Lett.*, Vol. 50, No. 10, 2561–2566, Oct. 2008.
9. Ma, J., S.-X. Gong, X. Wang, Y.-X. Xu, W.-J. Zhao, and J. Ling, "Efficient IE-FFT and PO hybrid analysis of antennas around electrically large platforms," *IEEE Antennas Wireless Propag. Lett.*, Vol. 10, 611–614, 2011.
10. Rao, S. M., D. R. Wilton, and A. W. Glisson, "Electromagnetic scattering by surfaces of arbitrary shape," *IEEE Trans. Antennas Propag.*, Vol. 30, No. 3, 409–418, May 1982.

11. Wan, J. X. and C.-H. Liang, "Rapid solutions of scattering from microstrip antennas using well-conditioned asymptotic waveform evaluation," *Progress In Electromagnetics Research*, Vol. 49, 39–52, 2004.
12. Ma, J., S.-X. Gong, X. Wang, Y. Liu, and Y.-X. Xu, "Efficient wide-band analysis of antennas around a conducting platform using MOM-PO hybrid method and asymptotic waveform evaluation technique," *IEEE Trans. Antennas Propag.*, Vol. 60, No. 12, 6048–6052, Dec. 2012.
13. Wang, X.-D. and D. H. Werner, "Improved model-based parameter estimation approach for accelerated periodic method of moments solutions with application to analysis of convoluted frequency selected surfaces and metamaterials," *IEEE Trans. Antennas Propag.*, Vol. 58, No. 1, 122–131, Jan. 2010.
14. Ling, J., S.-X. Gong, B. Lu, X. Wang, and W.-T. Wang, "Fast and accurate radar cross section computation using Chebyshev approximation in both broad frequency band and angular domains simultaneously," *Progress In Electromagnetics Research Letters*, Vol. 13, 121–129, 2010.
15. Ma, J., S.-X. Gong, X. Wang, P.-F. Zhang, and Z.-L. Lv, "Frequency sweep technology using Maehly approximation based on MOM-PO hybrid method," *Chinese Journal of Radio Science*, Vol. 28, No. 1, 45–49, 2013.
16. Dong, H.-L., S.-X. Gong, P.-F. Zhang, J. Ma, and B. Zhao, "Fast and accurate analysis of broadband RCS using method of moments with loop-tree basis functions," *IET Microw. Antennas & Propag.*, Vol. 9, No. 8, 775–780, 2015.